Molecular Therapy
Nucleic Acids
Brief report

Flow rate modulates focused ultrasound-mediated vascular delivery of microRNA

Stephanie He,[1] Davindra Singh,[1] and Brandon Helfield[1,2]

[1]Department of Biology, Concordia University, Montreal, QC H4B 1R6, Canada; [2]Department of Physics, Concordia University, Montreal, QC H4B 1R6, Canada

Gene therapy targeting ischemic heart disease is a promising therapeutic avenue, but it is mostly restricted to viral-based delivery approaches which are limited due to off-target immunological responses. Focused ultrasound presents a non-viral, image-guided technique in which circulating intravascular microbubble contrast agents can reversibly enhance vascular permeability and gene penetration. Here, we explore the influence of flow rate on the microbubble-assisted delivery of miR-126, a potent pro-angiogenic biologic, using a custom acoustically coupled pressurized mesenteric artery model. We demonstrate that under the same ultrasound conditions, increased flow rates enhance microbubble-mediated cell permeability; yet, miR-126 delivery itself exhibits a negative correlation with increasing flow velocity. Post-ultrasound assays confirmed vessel vasoreactivity, maintaining vasoconstriction and vasodilation capacities. These findings underscore the critical role microbubble flow rate plays in focused ultrasound gene therapy, especially notable for applications in which blood velocity itself is a salient pathophysiological indicator of disease progression, including ischemia.

INTRODUCTION

Despite ongoing advancements in specialized surgeries and pharmacotherapies,[1] ischemia and related cardiovascular diseases remain the leading causes of mortality.[2] Nucleic acid gene therapy is a rapidly advancing alternative to these approaches, and one of the most promising candidates for this technique in this disease context is microRNA-126 (miR-126), a strong regulator of angiogenesis.[3,4] Despite the initial success of miR-126 therapy, the lack of a safe and effective delivery method remains a significant challenge. Common strategies rely on viral vectors, which, while effective, carry the risk of eliciting dose-limiting immune responses and potential long-term safety concerns.[5]

Focused ultrasound and microbubbles have been extensively investigated as an alternative, non-viral approach to targeted gene delivery, addressing many of the limitations associated with other types of vectors. Microbubbles are small, gas-filled bubbles encapsulated often within a lipid shell. They remain entirely intravascular due to their size (1–8 μm in diameter) and are traditionally used as contrast agents in clinical imaging, particularly in cardiology.[6] When exposed to ultrasound, microbubbles oscillate and scatter nonlinear ultrasound energy that can be harnessed for contrast.[7] However, under specific acoustic conditions, they can be made to generate mechanical forces that temporarily increase the permeability of neighboring vasculature and cellular membranes.[8–11] This transient increase in permeability allows for the delivery of otherwise impermeable therapeutic agents, a technique that has made recent and significant advances in targeted blood-brain barrier permeation in the context of neurology and neuro-oncology,[12,13] and is rapidly expanding in the cardiovascular disease arena.[14]

The extent to which ultrasound-mediated microbubble vibrations permeate the surrounding vasculature, and the salient factors that affect its efficiency as a targeted therapeutic tool, is an expanding area of research. Chief among these factors is the microbubble flow rate, which has been shown recently to influence ultrasound-assisted endothelial cell membrane permeability enhancement[15] due, in part, to the local number density of bubbles passing through the acoustic beam per unit time, as well as the flow-regulated endothelial secretome.[16] Indeed, there is a paucity of information with respect to the relationship between flow velocity and enhanced drug/gene uptake. Notably, this is a critical parameter in the context of vascular stenosis, angiogenesis, arteriogenesis, and ischemia, where flow rate is expected to be modulated based on the extent and time course of disease.[17,18]

Here, we aim to explore how flow rate influences microbubble-assisted permeability and vascular delivery of pro-angiogenic miR-126 within a pressurized mesenteric artery model. With the development of this new model, we are able to additionally monitor vessel vasoactivity and vessel viability both before and after ultrasound exposure. After confirming viable vessel isolation, we assess the effect of increasing flow rate on microbubble-mediated cell permeability. We follow this with a subset of parallel experiments for the delivery of miR-126 under a range of acoustic conditions, and finally, we discuss our results within the broader context of focused ultrasound therapy.

Received 19 July 2024; accepted 10 December 2024;
https://doi.org/10.1016/j.omtn.2024.102426.

Correspondence: Brandon Helfield, Department of Biology, Concordia University, Montreal, QC H4B 1R6, Canada
E-mail: brandon.helfield@concordia.ca

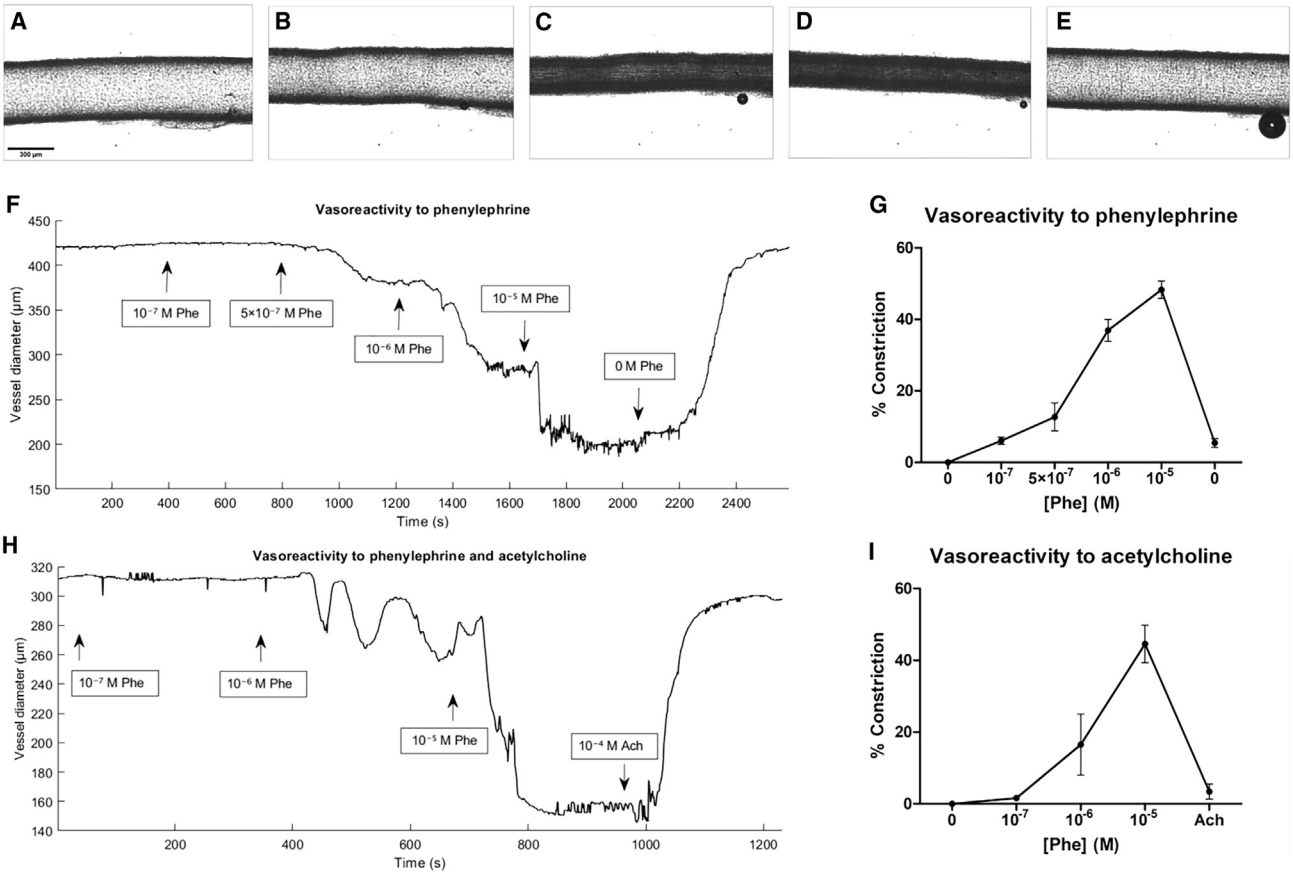

Figure 1. Viable extraction of third-order rat mesentery arteries

(A–E) Representative micrographs (see Video S1) of a pressurized vessel (60 mm Hg) responding to cumulative dosing of phenylephrine: (A) 0 M, (B) 5×10^{-7} M, (C) 10^{-6} M, (D) 10^{-5} M, and (E) 10^{-5} M and 10^{-4} M acetylcholine (Ach). Scale bar, 300 µm. (F–I) Sample vessel diameter versus time in response to either (F) phenylephrine-induced vasoconstriction alone or in combination with (H) acetylcholine-induced vasodilation and the (G and I) global summary of these vasoactivity assays. Arrows indicate when the doses were applied in (F) and (H). All data represented as mean ± SD, derived from at least $n = 3$ individual vessels per condition.

RESULTS

Our first objective was to confirm that our mesentery isolation and handling (Figure S1) yields viable vessels and to obtain a baseline of their vasoactive response. We performed two assays, phenylephrine-induced vasoconstriction and acetylcholine-induced vasodilation, representative examples of which are shown in Figures 1A–1H (see also Video S1). The global results are presented in Figures 1G–1I, in which the constriction percentage is reported (see the supplemental methods). Cannulated vessels obtain gradual vasoconstriction, reaching >40% constriction by 10^{-5} M phenylephrine ($p < 2.6e{-}6$ as compared to 0 M) and recovering up to >90% of its original diameter ($p < 0.003$ as compared to 0 M). Furthermore, recovery was observed under simultaneous 10^{-5} M phenylephrine and 10^{-4} M acetylcholine, corresponding to endothelium-dependent vasodilation. These levels of pressured vascular vasoconstriction and subsequent vasorelaxation are consistent with viable arteries reported elsewhere.[19,20]

We proceeded to incorporate clinical microbubble contrast agent Definity and a real-time membrane permeability marker (propidium iodide [PI]) within the perfusate. After confirmation of intravascular microbubbles (Figures 2A–2D; Video S2), the vessels were treated with ultrasound for 5 s (Figures 2E–2H, where the PI signal is shown in red). The complete dataset is summarized in Figures 2I–2K, where the relative number of PI^+ cells as compared to untreated sham controls as a function of flow rate is depicted under three ultrasound conditions (11.1%–44.4% duty cycles [DCs]). For the lowest acoustic setting, the number of permeabilized cells increased from 1.89- to 2.39-fold over control from 0.83–1.89 cm/s flow velocities (flow rates of 60–136 µL/min; see supplemental information), exhibiting a statistically significant increase between the slowest and fastest flow conditions ($p < 0.02$). When doubling the number of ultrasound cycles (22.2% DC), we observe a similar trend ranging from a 2.64- to 6.01-fold increase as compared to flow-matched controls ($p < 0.002$), and a 1.6- to 4.0-fold increase at 44.4% DC ($p < 0.02$). These conditions resulted in similar ultrasound-induced microbubble disruption (Figure S2). The control datasets here are vessels

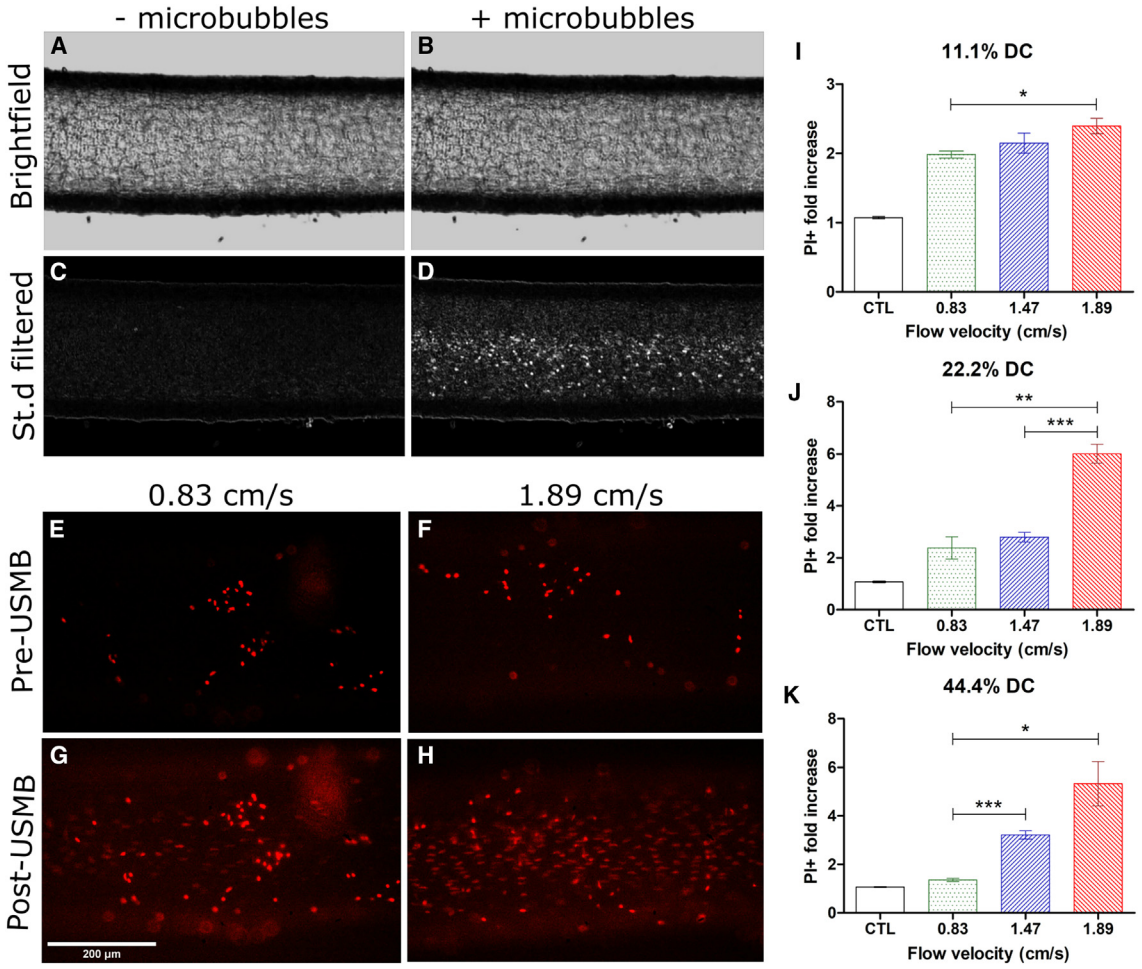

Figure 2. Vascular cell permeability increases with increasing microbubble flow rate

(A–D) Successful Definity entry into the vasculature was confirmed via bright-field microscopy (see Video S2). Representative bright-field micrograph of a vessel (A) without and (B) with microbubbles, along with SD-filtered processed versions to better delineate the flowing microbubbles (C and D). (E–H) Propidium iodide-positive (PI^+) cells before (E and F) and after (G and H) focused ultrasound treatments with an 11.1% duty cycle (DC) pulse under flow velocities 0.83 and 1.89 cm/s, respectively. (I–K) Quantification of flow-dependent cellular permeability, highlighting PI^+ fold increase within vessels treated at (I) 11.1% DC, (J) 22.2% DC, and (K) 44.4% DC at each of the flow velocities employed. All of the ultrasound-treated groups were statistically different from the control group, indicators of which were omitted to simplify the figure. Scale bar, 200 µm. $^*p < 0.05$; $^{**}p < 0.01$; $^{***}p < 0.001$.

that received ultrasound without the incorporation of contrast agent microbubbles.

While enhancing vascular cell membrane permeability is likely a necessary step for vascular gene delivery, it may not be sufficient. Thus, after confirming this flow rate-dependent bioeffect using Definity, our next objective consisted of delivering a relevant microRNA (pro-angiogenic miR-126) to the vascular tissue. Our results indicate that while ultrasound-assisted miR-126 delivery is also flow rate dependent at every acoustic condition employed here, the dependence on flow velocity is approximately opposite that of membrane perforation (Figure 3). Under an 11.1% DC treatment, we observe a 79-fold increase in miR-126 levels compared to sham and negative controls at the slowest flow rate (0.83 cm/s), with this level of delivery decreasing to 25-fold ($p < 0.003$ compared to slowest flow) and 51-fold ($p < 0.026$ compared to slowest flow; $p < 0.004$ compared to middle flow condition) at 1.47 cm/s and 1.89 cm/s, respectively (Figure 3A). This trend persisted as the DC increased to 22.2% (Figure 3B), whereby miR-126 levels increased 105-fold at 0.83 cm/s, 22-fold at 1.47 cm/s ($p < 0.007$ compared to slowest flow group), and 12-fold at 1.89 cm/s ($p < 0.004$ compared to slowest flow group). Finally, the stronger acoustic condition (44.4% DC) confirms this trend (Figure 3C), resulting in miR-126 levels of 23-fold at 0.83 cm/s, 17-fold at 1.47 cm/s ($p <$ not significant compared to slowest flow group) and 4-fold at 1.9 cm/s ($p < 0.01$ compared to slowest flow group).

To more easily compare the effect of the acoustic conditions, we summarize the data in Figure 3D, in which all three acoustic condition

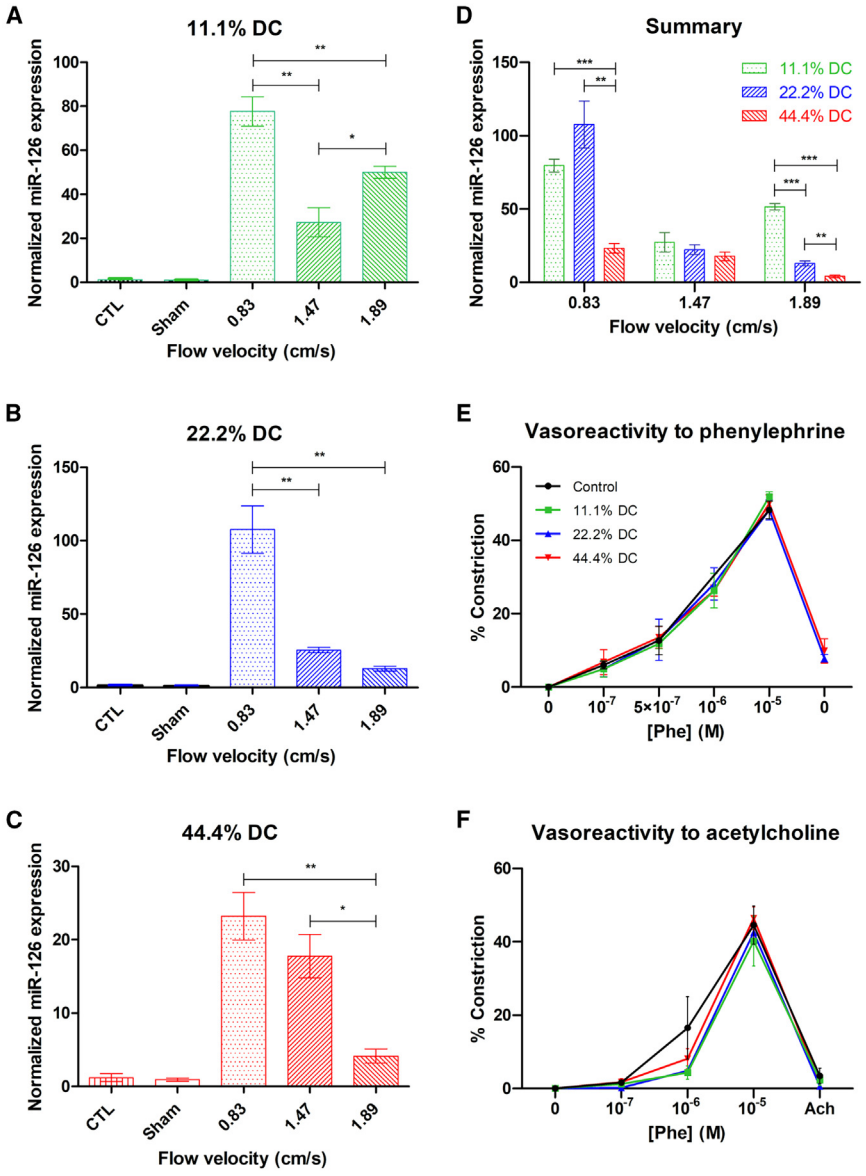

Figure 3. Focused ultrasound-mediated vascular delivery of miR-126 is flow dependent

(A–D) The delivery of miR-126 due to focused ultrasound treatments at (A) 11.1%, (B) 22.2%, and (C) 44.4% DC exposures. Data are represented as normalized to a housekeeping gene (see supplemental information). A global summary of miR-126 delivery as a function of flow velocity is shown in (D). (E and F) Phenylephrine-induced vasoconstriction assay (E) and (F) acetylcholine-induced vasodilation assay performed 30 min after focused ultrasound treatments at each DC regimen compared to the untreated controls ($n = 3$ for each), highlighting no loss of vessel viability. All of the focused ultrasound-treated groups were statistically different from the control (ultrasound with no miR-126) and sham (miR-126 but no ultrasound) groups, indicators of which were omitted to simplify the figure.

datasets are overlaid. Here, two interesting trends can be observed. First, as previously mentioned, there is an overall inverse relationship between microbubble flow velocity and miR-126 delivery. Second, at a given flow velocity, it is not directly the case that more ultrasound bursts (i.e., increasing DC) result in increased levels of miR-126 delivery. Both of these observations run contrary to the extent of plasma membrane permeability (Figures 2I–2K). Finally, we confirm vessel viability post-ultrasound therapy with all three acoustic regimes employed here (Figures 3E and 3F).

DISCUSSION

While the vast majority of mechanistic studies are performed on cell cultures under static microbubble conditions and different acoustic arrangements, the trend of increasing pulse duration resulting in increased plasma membrane permeability is generally an established one.[21–25] Perhaps more comparable, a limited number of studies have highlighted increased plasma membrane permeability under increasingly faster flow velocities when subjected to the same acoustic stimulus.[15] Faster microbubble velocity allows for more replenishment of new agents within the acoustic focus, and these are more likely to interact with the surrounding vessel tissue. In addition to a pure number density argument, microbubbles are known to respond differently as a function of burst length, including an increased propensity for acoustically driven disruption[26] and radiation force-induced bubble translation[27] with increasing pulse durations. While bubble translation serves to decrease the average distance between microbubbles and the vessel wall, it also serves to locally increase the microbubble concentration (i.e., secondary Bjerknes force[28]). This may trigger unique bubble-bubble interactions that are entirely dependent on the inter-bubble spacing,[29] in which bubbles that are usually non-responsive to the specific acoustic stimulus employed here become active and thus may additionally contribute to the observed bioeffects. While not directly observed here, these acoustic phenomena may explain the increased cell membrane perforation between the acoustic regimes at a given flow velocity. Finally, another aspect to consider is the susceptibility to mechanical perforation of the vasculature due to the differential flow-induced shear stress across the three flow velocities considered in this study. We have recently demonstrated in an endothelial monolayer model under flow conditions that shear-stress preconditioning can influence microbubble-assisted ultrasound-induced membrane perforation[16]—specifically that the shear-induced levels of cytokine secretion from endothelial cells may correlate with the propensity of ultrasound-assisted membrane

perforation. In regard to the vascular delivery of microRNA, the flow-dependent deposition of miR-126 (Figure 3) runs counterintuitively to the permeation data (Figure 2). Mechanistically, this may suggest that the molecular weight of the target biologic is a key factor in delivery efficiency under flow (668 g/mol vs. ~20,000 g/mol between PI and miR-126, respectively), the practical implications of which point to context-dependent ultrasound sequences and/or dosing paradigms.

We have demonstrated, for the first time, focused ultrasound-assisted gene delivery in a physiologically intact vessel and revealed its dependence on the flow rate of the perfusate. These results have implications for emerging focused ultrasound therapeutics spanning diseases that range in anatomical and pathophysiological flow conditions, including vascular stenosis and ischemia.

MATERIALS AND METHODS

See the supplemental information, which is available online (https://doi.org/10.1016/j.omtn.2024.102426).

DATA AND CODE AVAILABILITY

Data are available on request from the corresponding author.

ACKNOWLEDGMENTS

The authors acknowledge Seth Truran for his helpful guidance. This work was funded by the Canada Research Chairs program (CRC-2023-00137), the Canadian Cardiovascular Society (1512960), the Canadian Institutes of Health Research (PJT-190209), and the Fonds de Research du Quebec. B.H. is a Burroughs Wellcome Fund fellow (1018212.03).

AUTHOR CONTRIBUTIONS

S.H. conducted the experiments, and S.H., D.S., and B.H. designed the experiments. S.H. and B.H. analyzed the data, and all authors wrote and edited the paper.

DECLARATION OF INTERESTS

The authors declare no competing interests.

SUPPLEMENTAL INFORMATION

Supplemental information can be found online at https://doi.org/10.1016/j.omtn.2024.102426.

REFERENCES

1. Libby, P. (2021). The changing landscape of atherosclerosis. Nature *592*, 524–533. https://doi.org/10.1038/s41586-021-03392-8.

2. StatisticsCanada (2016). Table 102-0561 - Leading causes of death, total population, by age group and sex. CANSIM (database). https://doi.org/10.25318/1310039401-eng.

3. Schmidt, Y., Simunovic, F., Strassburg, S., Pfeifer, D., Stark, G.B., and Finkenzeller, G. (2015). MiR-126 regulates platelet-derived growth factor receptor-α Expression and migration of primary human osteoblasts. Biol. Chem. *396*, 61–70. https://doi.org/10.1515/hsz-2014-0168.

4. Schober, A., Nazari-Jahantigh, M., Wei, Y., Bidzhekov, K., Gremse, F., Grommes, J., Megens, R.T.A., Heyll, K., Noels, H., Hristov, M., et al. (2014). MicroRNA-126-5p promotes endothelial proliferation and limits atherosclerosis by suppressing Dlk1. Nat. Med. *20*, 368–376. https://doi.org/10.1038/nm.3487.

5. Zhao, Z., Anselmo, A.C., and Mitragotri, S. (2022). Viral vector-based gene therapies in the clinic. Bioeng. Transl. Med. *7*, e10258. https://doi.org/10.1002/btm2.10258.

6. Lindner, J.R. (2004). Microbubbles in medical imaging: current applications and future directions. Nat. Rev. Drug. Discov. *3*, 527–532. https://doi.org/10.1038/nrd1417.

7. Helfield, B. (2019). A review of phospholipid encapsulated ultrasound contrast agent microbubble physics. Ultrasound Med. Biol. *45*, 282–300. https://doi.org/10.1016/j.ultrasmedbio.2018.09.020.

8. Helfield, B., Chen, X., Watkins, S.C., and Villanueva, F.S. (2016). Biophysical insight into mechanisms of sonoporation. Proc. Natl. Acad. Sci. USA *113*, 9983–9988. https://doi.org/10.1073/pnas.1606915113.

9. Helfield, B., Chen, X., Watkins, S.C., and Villanueva, F.S. (2020). Transendothelial Perforations and the Sphere of Influence of Single-Site Sonoporation. Ultrasound. Med. Biol. *46*, 1686–1697. https://doi.org/10.1016/j.ultrasmedbio.2020.02.017.

10. Hu, Y., Wan, J.M.F., and Yu, A.C.H. (2013). Membrane perforation and recovery dynamics in microbubble-mediated sonoporation. Ultrasound Med. Biol. *39*, 2393–2405. https://doi.org/10.1016/j.ultrasmedbio.2013.08.003.

11. Skyba, D.M., Price, R.J., Linka, A.Z., Skalak, T.C., and Kaul, S. (1998). Direct in vivo visualization of intravascular destruction of microbubbles by ultrasound and its local effects on tissue. Circulation *98*, 290–293. https://doi.org/10.1161/01.CIR.98.4.290.

12. Meng, Y., Reilly, R.M., Pezo, R.C., Trudeau, M., Sahgal, A., Singnurkar, A., Perry, J., Myrehaug, S., Pople, C.B., Davidson, B., et al. (2021). MR-guided focused ultrasound enhances delivery of trastuzumab to Her2-positive brain metastases. Sci. Transl. Med. *13*, eabj4011.

13. Abrahao, A., Meng, Y., Llinas, M., Huang, Y., Hamani, C., Mainprize, T., Aubert, I., Heyn, C., Black, S.E., Hynynen, K., et al. (2019). First-in-human trial of blood–brain barrier opening in amyotrophic lateral sclerosis using MR-guided focused ultrasound. Nat. Commun. *10*, 4373. https://doi.org/10.1038/s41467-019-12426-9.

14. Singh, D., Memari, E., He, S., Yusefi, H., and Helfield, B. (2024). Cardiac gene delivery using ultrasound: State of the field. Mol. Ther. Methods Clin. Dev. *32*, 101277. https://doi.org/10.1016/j.omtm.2024.101277.

15. Memari, E., Hui, F., Yusefi, H., and Helfield, B. (2023). Fluid flow influences ultrasound-assisted endothelial membrane permeabilization and calcium flux. J. Contr. Release *358*, 333–344. https://doi.org/10.1016/j.jconrel.2023.05.004.

16. Memari, E., and Helfield, B. (2024). Shear stress preconditioning and microbubble flow pattern modulate ultrasound-assisted plasma membrane permeabilization. Mater. Today. Bio *27*, 101128. https://doi.org/10.1016/j.mtbio.2024.101128.

17. Messina, L.M., Brevetti, L.S., Chang, D.S., and Paek, R. (2002). Therapeutic angiogenesis for critical limb ischemia: invited commentary. J. Contr. Release *78*, 285–294.

18. Annex, B.H., and Cooke, J.P. (2021). New Directions in Therapeutic Angiogenesis and Arteriogenesis in Peripheral Arterial Disease. Circ. Res. *128*, 1944–1957. https://doi.org/10.1161/CIRCRESAHA.121.318266.

19. Wenceslau, C.F., McCarthy, C.G., Earley, S., England, S.K., Filosa, J.A., Goulopoulou, S., Gutterman, D.D., Isakson, B.E., Kanagy, N.L., Martinez-Lemus, L.A., et al. (2021). Guidelines for the measurement of vascular function and structure in isolated arteries and veins. Am. J. Physiol. Heart. Circ. Physiol. *321*, H77–H111. https://doi.org/10.1152/ajpheart.01021.2020.

20. Lu, X., and Kassab, G.S. (2011). Assessment of endothelial function of large, medium, and small vessels: a unified myograph. Am. J. Physiol. Heart Circ. Physiol. *300*, 94–100. https://doi.org/10.1152/ajpheart.00708.2010.-Endothelial.

21. Tu, J., and Yu, A.C.H. (2022). Ultrasound-Mediated Drug Delivery: Sonoporation Mechanisms, Biophysics, and Critical Factors. BME Front. *2022*, 9807347. https://doi.org/10.34133/2022/9807347.

22. Han, Y.W., Ikegami, A., Chung, P., Zhang, L., and Deng, C.X. (2007). Sonoporation is an efficient tool for intracellular fluorescent dextran delivery and one-step double-crossover mutant construction in Fusobactenum nucleatum. Appl. Environ. Microbiol. *73*, 3677–3683. https://doi.org/10.1128/AEM.00428-07.

23. Pan, H., Zhou, Y., Izadnegahdar, O., Cui, J., and Deng, C.X. (2005). Study of sonoporation dynamics affected by ultrasound duty cycle. Ultrasound Med. Biol. *31*, 849–856. https://doi.org/10.1016/j.ultrasmedbio.2005.03.014.

24. Navarro-Becerra, J.A., Caballero-Robledo, G.A., Franco-Urquijo, C.A., Ríos, A., and Escalante, B. (2020). Functional Activity and Endothelial-Lining Integrity of Ex Vivo

Arteries Exposed to Ultrasound-Mediated Microbubble Destruction. Ultrasound Med. Biol. *46*, 2335–2348. https://doi.org/10.1016/j.ultrasmedbio.2020.05.004.

25. Hallow, D.M., Mahajan, A.D., and Prausnitz, M.R. (2007). Ultrasonically targeted delivery into endothelial and smooth muscle cells in ex vivo arteries. J. Control. Release. *118*, 285–293. https://doi.org/10.1016/j.jconrel.2006.12.029.

26. Chomas, J.E., Dayton, P., May, D., and Ferrara, K. (2001). Threshold of fragmentation for ultrasonic contrast agents. J. Biomed. Opt. *6*, 141–150. https://doi.org/10.1117/1.1352752.

27. Dayton, P.A., Allen, J.S., and Ferrara, K.W. (2002). The magnitude of radiation force on ultrasound contrast agents. J. Acoust. Soc. Am. *112*, 2183–2192. https://doi.org/10.1121/1.1509428.

28. Crum, L.A. (1975). Bjerknes forces on bubbles in a stationary sound field. J. Acoust. Soc. Am. *57*, 1363–1370.

29. Yusefi, H., and Helfield, B. (2022). The influence of inter-bubble spacing on the resonance response of ultrasound contrast agent microbubbles. Ultrason. Sonochem. *90*, 106191. https://doi.org/10.1016/j.ultsonch.2022.106191.